Surface structures from NH_3 chemisorption in CVD and ALD of AlN, GaN and InN films

Karl Rönnby*, Henrik Pedersen, and Lars Ojamäe

Department of Physics, Chemistry and Biology (IFM), Linköping University

*Corresponding author: karl.ronnby@liu.se

Abstract

Aluminum nitride (AlN), gallium nitride (GaN) and indium nitride (InN) form a family of technologically important semiconductors of high importance to light-emitting diodes and high frequency electronics. Although thin films of these materials are routinely manufactured by chemical vapor deposition (CVD) and atomic layer deposition (ALD), the methods are far from optimal and knowledge of the underlaying chemical processes are lacking. In this work we performed *ab-initio* investigations of the surface coverage of these materials under an ammonia rich atmosphere. Periodic density functional theory (DFT) calculations were used to test probable surface structures, their electronic and thermal energies were used to calculate their contribution to the surface composition at temperature and pressure conditions relevant for CVD and ALD processes of these materials. The results show similarities between the group of materials with similar NH_x surface structure present for all three. Comparison of the coverage showed that at low growth temperatures the surface is expected to be covered by NH_2 while at high temperatures most surface sites would be vacant. The surface structures where all found to be most stable on AlN and least stable on InN. These results are important for further investigations of the material growth mechanisms.

Introduction

The group 13 nitrides (13Ns), aluminum (AlN), gallium (GaN) and indium nitride (InN) are important materials in the semiconductor industry [1]. They range in bandgap from the wide gap of 6.0 eV for AlN [2], to the narrow 0.7 eV for InN [3] with GaN at an intermediate gap of 3.4 eV [4]. This bandgap range covers ultra-violet to infra-red and thus contains the full visible spectrum making the 13Ns well suited for optoelectronics such as LEDs [5,6]. InN has also a very high electron mobility and electron saturation velocity making it suited for high frequency transistors [7,8].

To use the 13Ns in these applications they need to form thin films with high crystalline quality, conformity, and low impurity levels. One common method to achieve such films for AlN and

GaN is chemical vapor deposition (CVD). CVD of AlN and GaN is routinely done at temperatures around 800-1100 °C. For InN, conventional CVD is problematic to use as InN decomposes into metallic indium and nitrogen gas at around 500 °C [1], well below the temperatures needed to activate the decomposition chemistry of ammonia which is used as nitrogen precursor in the growth process [9]. Atomic layer deposition (ALD) is a low temperature CVD method with a time-resolved supply of the precursors, leading to a deposition fully governed by surface chemical reactions. ALD has the potential to circumvent the high temperature required in CVD of 13Ns and at the same time increase the ability to uniformly coat substrates with very high aspect ratios. ALD has already been demonstrated to be superior to continuous CVD for deposition of the temperature sensitive InN films [10,11].

Insight from modeling can be used to better understand the surface chemical processes in ALD and CVD. One of the foundations for the surface chemistry are the surface structures of the substrates covered with the adsorbates. From the possible surface terminations of the 13Ns, the reactivity of the different possible surfaces can be estimated. The surface structures are also needed to be able to investigate adsorption pathways as well as adatom diffusion. Earlier theoretical studies of NH_3 adsorption and decomposition on GaN [12,13] and InN [13,14] have shown that NH_3 can decompose into a variety of NH_x adatoms upon adsorption on the 13Ns, often with surface NH_2 being one of the most prominent species. The adsorption and decomposition on AlN have not previously been investigated in detail.

Most of the studies are performed at a low coverage with only a single or few NH_x adatoms in the computational cell giving a coverage of up to around 0.25 ML. At higher coverage, lateral effects can modify the structures and shift the surface energies, changing which configuration is the most favorable. The structures from the earlier works were used as a basis and we extend them by increasing the coverage to the limiting 1 ML as expected by a complete ALD process. We further extend these works by comparing the possible adsorbate-surface structures in the whole family of 13Ns as well as employing a statistical mechanical approach investigate the mixing of the different surface-coverage structures and view the dependence of the mixing on temperature, gas mixture and pressure. We find that the most probable surface NH_x specie at low temperatures is the on-top NH_2 for AlN, GaN and InN. At high temperatures, no NH_x species are stable on the surface and will desorb, leaving a bare surface. The transition temperatures between these two follows a clear trend where AlN has the highest transition temperature and InN the lowest with GaN in between.

Computational method

Quantum chemical calculation

All quantum chemical calculations were performed using density functional theory (DFT) as implemented in the VASP software [15–17], extended by the VTST package [18]. Electronic energies, geometry optimized structures and normal vibrations were all calculated using the GGA functional PBE [19] with Grimme's version 3 dispersion correction [20]. A plane wave basis set and the projector augmented wave method (PAW) [21] were used for core electrons. For Ga and In, 3d and 4d-electrons respectively were treated as valence electrons. To model the surface, a slab of each respective 13N compound was made from an optimized unit cell. First the unit cell was reoriented to make a conventional cell with axis along the $[10\bar{1}0]$ and $[1\bar{2}10]$ direction, containing 4 primitive cells. The conventional cell was then repeated in the $[0001]$ direction and padded with vacuum. The number of layers and vacuum separation as well as cut-off energy and number of k-points were checked to be converged with respect to the surface energy. Dangling bonds on the bottom of the slab were passivated by hydrogen atoms to limit artificial charges across the slab and vacuum padding.

During optimization, all atoms were allowed to relax, and the optimization criteria was set to 0.01 eV/Å. Normal mode frequencies were calculated using the harmonic approximation and the finite displacement method were used to get the force constants using the Phonopy software [22]. During frequency calculations, the atoms below the 2nd topmost layer were frozen. The normal mode frequencies were then used to calculate the vibrational part of the partition function and used to get thermodynamic properties for the surface system.

Calculations on gas phase molecules were performed by placing the molecule in a cubic cell with side 10 Å to ensure separation from the neighboring cells. For gaseous molecules, modes corresponding to translational and rotational movement were removed from the vibrations and the translational and rotational contributions to the partition function were calculated separately. These were then, together with the vibrational contribution, used to get the thermochemical properties of the molecules.

Equilibrium composition calculation

According to statistical mechanics, a system in the isothermal-isobaric ensemble will minimize its Gibbs energy (eq. 1) at equilibrium.

$$G(\boldsymbol{n}) = \sum_i \mu_i n_i \,, \tag{1}$$

where the summation goes over all species defined to be present in the system.

This gives an optimization problem for the equilibrium composition

$$\underset{\boldsymbol{n}}{\text{minimize}}\, G(\boldsymbol{n}) \tag{2}$$

subject to $A\boldsymbol{n} = \boldsymbol{b}$ and $n_i \geq 0$ where A is the matrix of the elemental composition of the species and $\boldsymbol{b}$ is a vector of the amount of the elements. The chemical potential was calculated using the Gibbs energy of the pure species at the total pressure p° (μ_i°) and the chemical activity (a_i) as the sum

$$\mu_i = \mu_i^\circ + RT \ln a_i \,. \tag{3}$$

For gas species the activity was approximated by the partial pressure $a_i = \frac{p_i}{p^\circ}$ while for surface species the activity was defined as the coverage ratio $a_i = \frac{n_i}{n_{tot}}$. The Gibbs energies of the pure species were calculated from the partition function derived from the quantum chemical calculations. Optimization were performed using Optimization Toolbox from Matlab R2021a.

Results

Adsorption of NH_x species and surface reconstructions

To investigate the different possible surface structures of 13Ns under an ammonia ambient atmosphere, NH_x (x=0-3) molecules or radicals were introduced to the surface slab. The NH_x species were placed in proximity of possible adsorption sites and the structures were optimized to find stable adsorption configurations. The four different adsorption sites considered, viewed along the (0001) axis, were: top (directly above a metal site), bridge (between two neighboring metal sites), hcp hollow (between three neighboring metal sites, above the top layer nitrogen), and fcc hollow (between three neighboring metal sites, above the empty site in hexagonal packing), see Figure 1. No adsorbate was found to adsorb to the hcp hollow site, probably due to the close proximity to, and repulsion from, the surface layer nitrogen. As a model for the possible surface after an ideal ALD half cycle, reconstructions were investigated assuming a 1:1 coverage between NH_x and surface metal sites if possible. Most of the investigated reconstructions were very similar for the different 13Ns with only small differences in bond lengths and angles, their structures are discussed in the following sections.

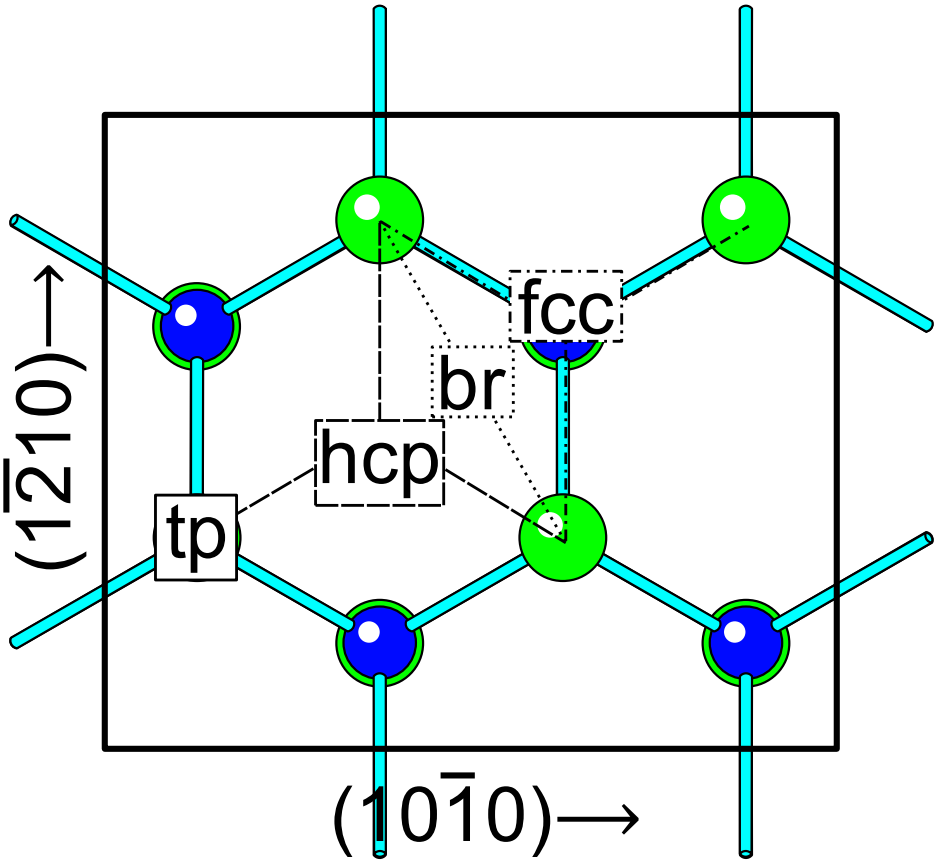

Figure 1. The four different adsorption sites, viewed along the (0001) axis; tp: top, directly above a metal (green atom) site, br: bridge, between two neighboring metal sites, hcp: hcp hollow, between three neighboring metal sites above the top layer nitrogen (blue atom) and fcc: fcc hollow, between three neighboring metal sites above the empty site in hexagonal packing.

NH_3 adsorption structure

Undecomposed NH_3 was found to adsorb on the top site, Figure 2. After a coverage of 0.5 monolayer of NH_3, additional NH_3 only weakly physisorb at a large distance above the surface layer. This can be seen as a saturation of the NH_3 coverage, since when an ammonia molecule binds to a metal site, it will contribute with two valence electrons to the surface metals. At a 0.5 ML NH_3 coverage, the number of valence electrons will form a full octet for each surface metal by forming a bond to the ammonia on half of the sites and a free electron pair on the other half. This free electron pair would then in turn repel the free pair of additional NH_3 causing them not to adsorb.

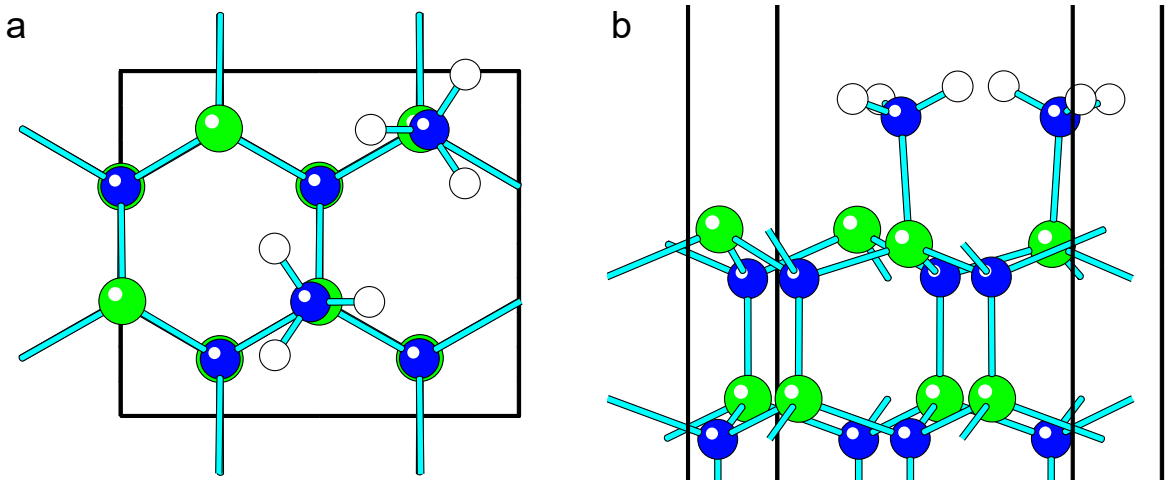

Figure 2. Top (a) and side (b) view of NH_3 adsorption at 0.5 ML coverage on AlN. Green atoms are Aluminum, blue are Nitrogen and while are Hydrogen.

NH_2 adsorption structures

From geometry optimization of surface structures fully covered by NH_2, two possible surface reconstructions were found on all three 13Ns surfaces, Figures 3, 4, S1 and S3. In the first reconstruction, the NH_2 groups are situated at the top adsorption site above the metal site, Figures 3 and S1. The bond lengths between the groups and metal sites for this structure are shorter than the bonds for bridging NH_2, 1.85 Å for AlN, 1.91 Å for GaN and 2.15 for InN. The groups are angled so that one of the hydrogen atoms points directly towards the lone electron pair on the nitrogen atom on a neighboring group forming a hydrogen bond between the groups with R(H···N) bond lengths at 2.08 Å for AlN, 2.09 Å for GaN and 2.36 for InN. By aligning the NH_2 groups with every other rotated by 120°, a zig-zag pattern of hydrogen bonds is formed over the surface maximizing the amount of hydrogen bonds, allowing each group to both donate and accept a hydrogen bond, Figure S2. Due to attraction caused by the hydrogen bonds the NH_2 groups are folded from the straight on top site in the direction of the bond by 4° for AlN, 5° for GaN and 7° for InN. The presence of an unguarded lone pair on the nitrogen atom makes it possible for a metal precursor, such as trimethyl group 13 metals (TM13), to form a Lewis adduct with the surface. This makes the structure a strong candidate for adsorption sites for the metal precursors.

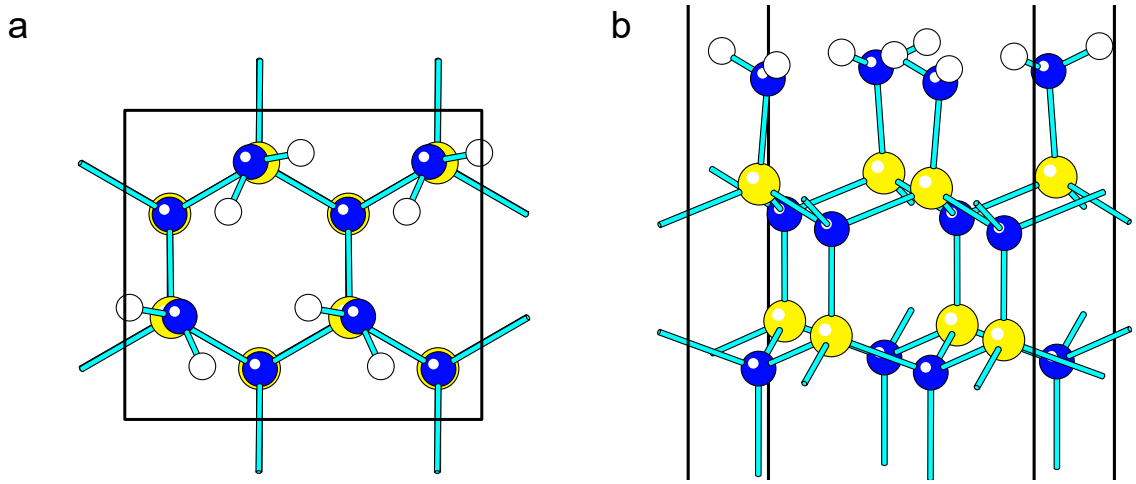

Figure 3. Top (a) and side (b) view of top NH_2 adsorption on GaN. Yellow atoms are Gallium, blue are Nitrogen and while are Hydrogen.

The second structure has the NH_2 groups positioned at the bridging site between two neighboring metal sites with the hydrogen atoms perpendicular to the bridge, Figures 4 and S3. Each metal site binds to two bridging NH_2 on alternate sides forming parallel rows along the surface. While the NH_2 groups are positioned at equal distance from the two metal sites the bond distances between the metal site and the nitrogen atom in the NH_2 groups increases as the metal atom goes down in the group (2.14 Å for AlN, 2.20 Å for GaN and 2.39 Å for InN). The NH_2 groups are shifted slightly from the line between the metal sites towards the hollow site, which could be due to repulsion from the nitrogen atom in the topmost surface layer. The angel of the bonds between the nitrogen of the NH_2 group and the surface sites to the (0001) direction are 43° for both AlN and GaN and 41° for InN, showing that the groups are drawn close to the surface. The closeness to the surface together with the lack of any free electron pair on the nitrogen would make it hard for a metal precursor to find an adsorption site, without the surface reconstructing further.

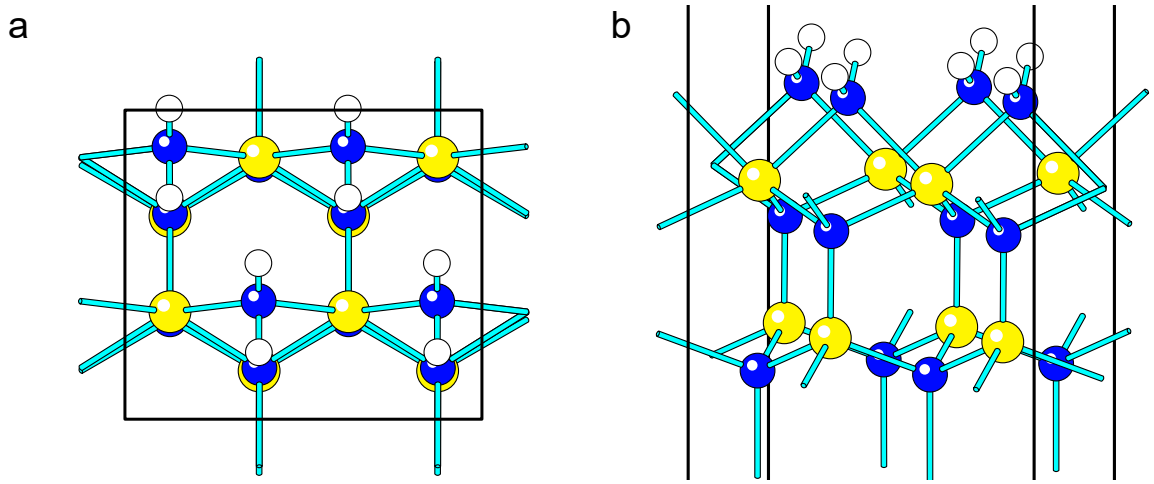

Figure 4. Top (a) and side (b) view of bridging NH_2 adsorption on GaN. Yellow atoms are Gallium, blue are Nitrogen and while are Hydrogen.

NH adsorption structures

When the structure was fully covered by NH, the geometry optimization also resulted in two possible structures for all three 13Ns, Figures 5-7 and S4-S6. In one of the reconstructions (Figures 5 and S4), the NH groups are located at the hollow site bridging all three surface metal atoms at equal distance (2.04 Å for AlN, 2.08 Å for GaN and 2.29 Å for InN). The hydrogen atoms in the groups are positioned right above the nitrogen, giving the group an almost tetrahedral geometry. The group is drawn very close to the surface layer, the angle between bond and the (0001) plane being only 28º for AlN, 27° for GaN and 26° for InN. This together causes the structure to be quite strained and thus a more unlikely surface structure.

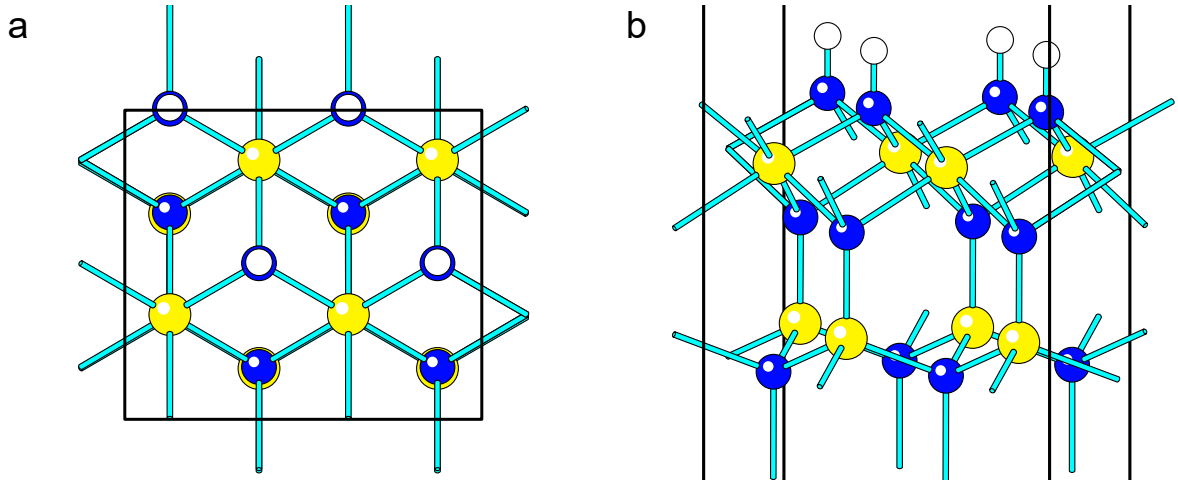

Figure 5. Top (a) and side (b) view of hollow NH adsorption on GaN. Yellow atoms are Gallium, blue are Nitrogen and while are Hydrogen.

The other structure is the combination of two neighboring NH groups into a $(NH)_2$ dimer, Figures 6, 7, S5 and S6. There exist two slightly different configurations for the dimer structures, the dimer could either bind in the hollow (Figures 6 and S5) or bridging site (Figures 7 and S6). On AlN, only the hollow site is a stable binding site for the dimer, while for GaN and InN both the bridging and the hollow binding sites are available. In the hollow position, the dimer binds with one of the nitrogen atoms to one to the three metal sites around the hollow site, with a bond length of 1.91 Å for AlN, 1.97 Å for GaN and 2.22 for InN. The other nitrogen bridges the two other metal sites around the hollow site with one covalent and one slightly longer coordinating bond, 2.10 and 2.25 Å for AlN, 2.19 and 2.29 Å for GaN and 2.45 and 2.55 Å for InN. The bond length between the two nitrogen atoms in the dimer becomes shorter as the atomic number of the metal increases (1.44 Å for AlN, 1.43 Å for GaN and 1.38 Å for InN), going from hydrazine like (1.46 Å) to diimide like (1.25 Å) indicating an increase of bond strength between the nitrogen in the dimer. The torsion of the two hydrogen atoms around the N-N bond is 49° for AlN, 54° for GaN and 31° for InN showing that the dimer is in a somewhat staggered conformation for AlN and GaN, while for InN the dimer is in the middle between eclipsed and staggered configuration. The dimer has one free electron pair pointing away from the surface allowing it to participate in Lewis adducts and could thus be a nucleation point for metal precursors.

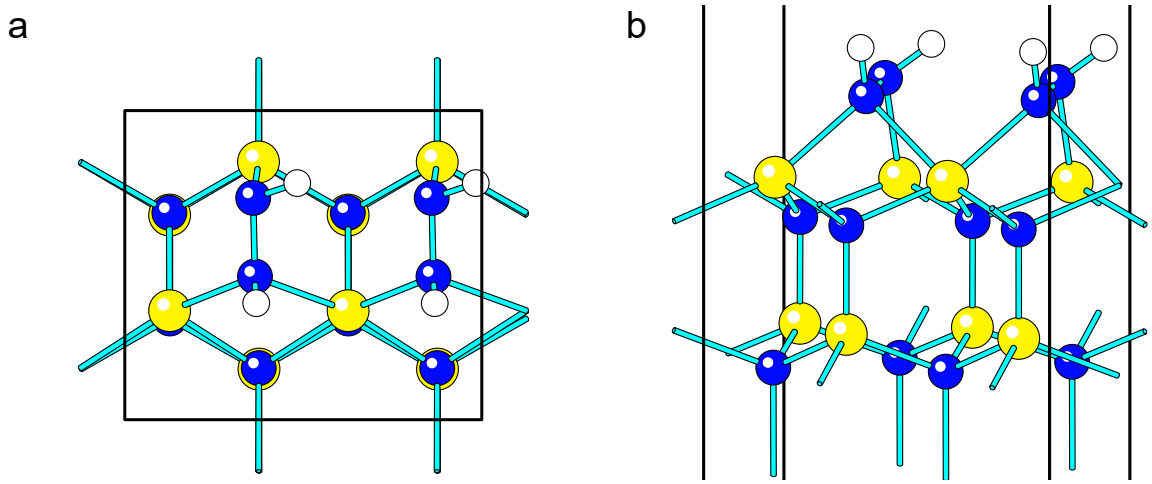

Figure 6. Top (a) and side (b) view of hollow N_2H_2 adsorption on GaN. Yellow atoms are Gallium, blue are Nitrogen and while are Hydrogen.

In the bridging configuration, the two nitrogen atoms in the dimer binds to two neighboring metal sites with bond lengths of 1.98 Å for GaN and 2.26 Å for InN. The two bonds are of the same length. As with the dimer at the hollow site, the N-N bond is longer for GaN (1.42 Å) than for InN (1.38 Å), again showing a transition from a hydrazine to a diimide like bond. Both

hydrogen atoms lay on the same side of the N-N bond giving the dimer a slightly eclipsed torsion at 17° for both GaN and InN. The lone electron pairs on both nitrogen atoms are unguarded and can thus serve as an adsorption site for a group 13 precursor via Lewis adduct formation.

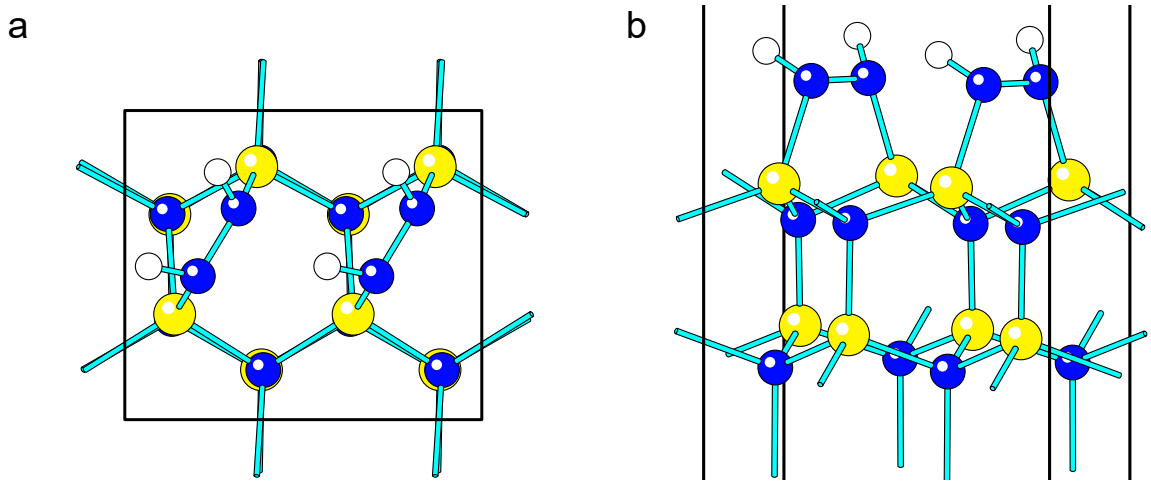

Figure 7. Top (a) and side (b) view of bridging N_2H_2 adsorption on GaN. Yellow atoms are Gallium, blue are Nitrogen and while are Hydrogen.

N adsorption structures

Full coverage of N atoms was also investigated, and similar to the NH terminated surfaces N terminations was also found to form both N monomer and N_2 dimers on the surface. The N monomer, Figures 8 and S7, was found to bind to the hollow site with three equal bonds to the closest metal sites (2.06 Å for AlN, 2.09 Å for GaN and 2.29 Å for InN). The presence of unpaired electrons causes the reconstruction to be a reactive surface and would easily decompose into other terminations.

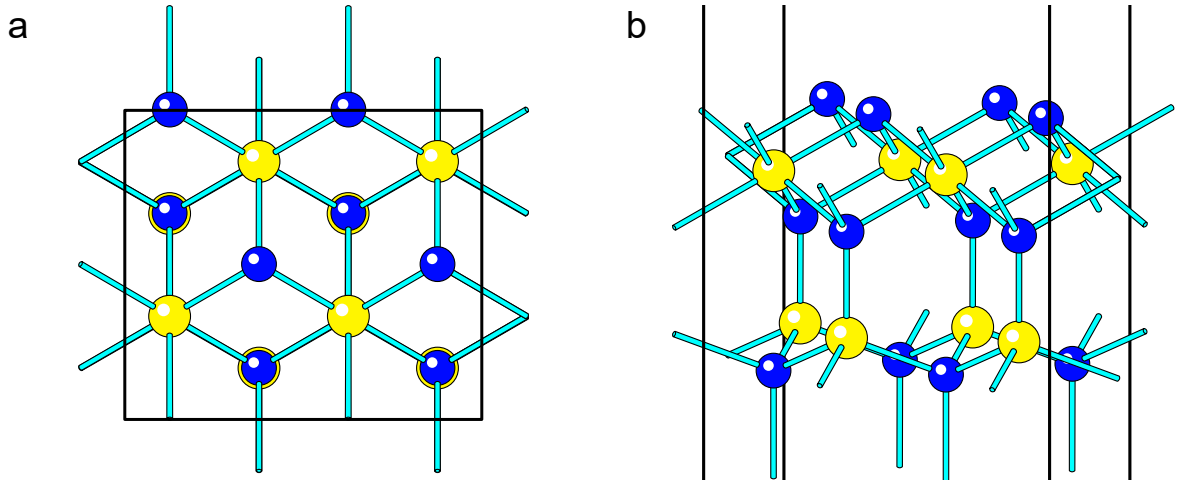

Figure 8. Top (a) and side (b) view of hollow N adsorption on GaN. Yellow atoms are Gallium, blue are Nitrogen and while are Hydrogen.

As with the N_2H_2 dimer, the N_2 dimer also has two different configurations in which the dimer is either at the hollow or at the bridging site, Figures S8 and 9. For AlN the only reconstruction possible is with the dimer in the hollow site. In this configuration one of the N atoms binds to a single metal site with bond length 1.91 Å, while the other N atom binds to the two other metal sites around the hollow site with almost equal bond length (2.10 and 2.25 Å). This causes the adatom to be forced into a bucking configuration with the single bonded nitrogen raised further from the surface than the double bonded. For GaN only the bridging dimer is possible, where the dimer is placed between two surface metal sites, with bonds of 2.18-2.21Å. The N-N bond (1.221 Å for AlN and 1.182 for GaN) is slightly shorter than a N=N double bond distance indicating it still has some character of the triple bond of molecular nitrogen and thus the electrons are not fully shifted to the surface bonds and becomes shorter as the atomic number of the metal increases. On InN the N_2 dimer does not stay chemisorbed to the surface and instead is only weakly physiosorbed at a large distance to the surface (> 4 Å). The surface form a structure very similar to the structure of a bare InN surface.

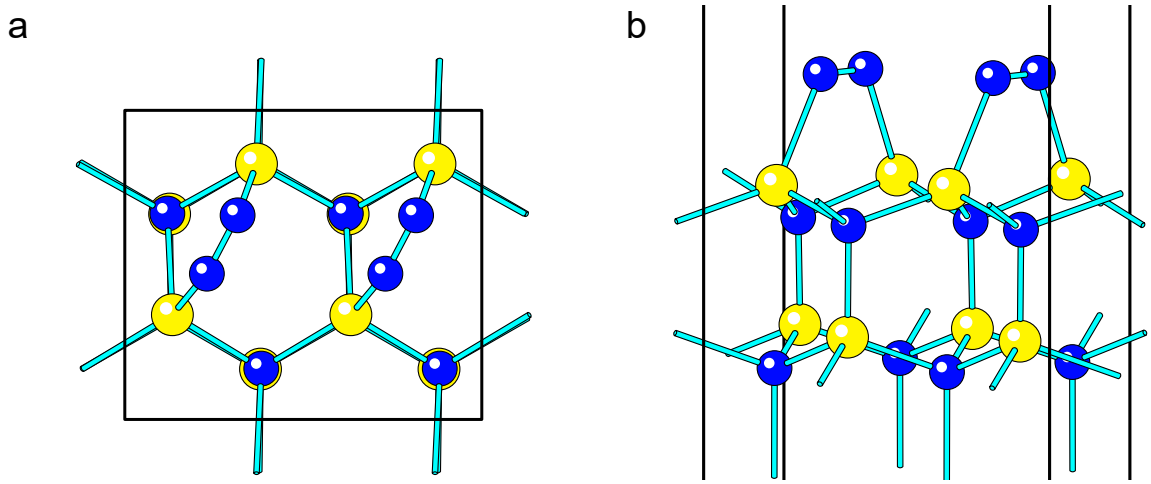

Figure 9. Top (a) and side (b) view of bridging N_2 adsorption on GaN. Yellow atoms are Gallium, blue are Nitrogen and while are Hydrogen.

Other adsorption structures

Structures for two other terminations were also investigated; a surface terminated by H, Figures 10 and S9, and a surface with no termination, Figures 11 and S10. For all 13Ns with H terminated surfaces, the hydrogen adatoms adsorbed on the top site with a bond length of 1.62 Å for AlN, 1.55 Å for GaN and 1.73 Å for InN.

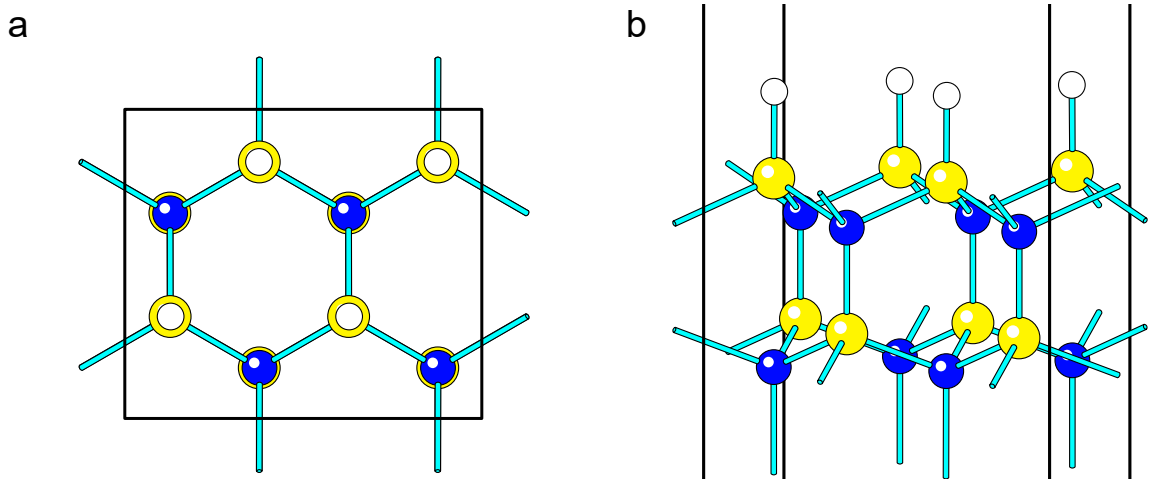

Figure 10. Top (a) and side (b) view of top H adsorption on GaN. Yellow atoms are Gallium, blue are Nitrogen and while are Hydrogen.

For AlN the bare surface underwent very lite reconstruction, the bond lengths between the surface atoms and the atoms in the 2nd layer are very close to the bulk distances. GaN and InN on the other hand reconstructed in a 2x1 manner, in which every other metal atom was moved downwards giving them an almost planar sp^2-like configuration while the other metal atoms stayed in a tetrahedral sp^3-like configuration. This allows the electrons from the dangling bonds

to pair up and lowers the magnetic moment significantly compared to the unreconstructed surface. These reconstructions are in agreement with previous findings [14,23].

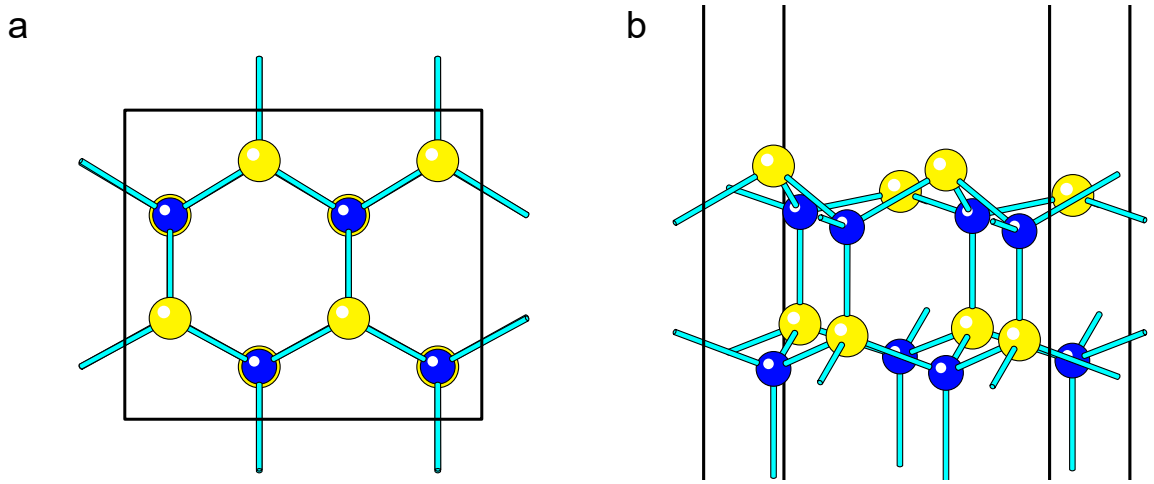

Figure 11. Top (a) and side (b) view of bare GaN. Yellow atoms are Gallium, blue are Nitrogen and while are Hydrogen.

Standard energy of the adsorbate

To be able to compare the adsorption energies for the different species, the standard formation energies of the adsorbate was calculated as

$$\Delta_{ads}E = E_{N_nH_m(ads)} - \left(E_{vacant} + \frac{n}{2}E_{N_2(g)} + \frac{m}{2}E_{H_2(g)}\right) \quad (4)$$

were $E_{N_nH_m(ads)}$ is the energy of the adsorbed species per site, E_{vacant} is the energy of the vacant surface per site and $E_{H_2(g)}$ and $E_{N_2(g)}$ is the energy of hydrogen and nitrogen molecules in gas phase. As the energy is given per surface site Equation 4 was used to calculate the electronic energy ($\Delta_{ads}E^{elec}$), enthalpy ($\Delta_{ads}H°$), free energy ($\Delta_{ads}G°$) and heat capacity ($\Delta_{ads}c_p$) of adsorption. The calculated energies are listed in Table I.

Table I. Standard energies of adsorption at STP (298.15 K and 1 bar). If the structure is not a minimum on the electronic-energy surface it is marked by a hyphen in the table.

	NH_2(tp)	NH_2(br)	NH(ho)	N_2H_2(ho)	N_2H_2(br)	N(ho)	N_2(ho)	N_2(br)	H(tp)
Electronic energy (kJ mol^{-1})									
AlN	-253.9	-213.9	-25.2	-146.5	—	197.9	-52.6	—	-65.8
GaN	-197.3	-146.6	53.4	-82.3	-69.2	264.4	—	-12.5	-67.8
InN	-115.9	-108.4	91.7	-22.9	-15.8	296.5	—	—	-5.2
Enthalpy (kJ mol^{-1})									
AlN	-226.5	-187.5	-16.9	-131.0	—	194.0	-51.0	—	-65.0
GaN	-170.4	-121.3	38.8	-67.5	-55.3	261.0	—	-11.7	-65.3
InN	-91.4	-84.4	99.3	-9.6	-2.2	293.1	—	—	-5.6
Gibbs free energy (kJ mol^{-1})									
AlN	-163.9	-126.3	24.0	-85.4	—	215.3	-26.1	—	-46.0
GaN	-107.4	-58.9	80.8	-21.8	-10.2	283.9	—	12.6	-45.1

InN	-33.0	-25.0	140.1	33.3	40.9	315.8	—	—	13.0
Heat capacity (J mol^{-1} K^{-1})									
AlN	-15.8	-12.3	1.2	-10.9	—	9.0	0.2	—	-5.5
GaN	-15.5	-13.6	-3.3	-9.9	-10.5	7.8	—	-0.2	-6.1
InN	-9.6	-8.1	1.7	-6.0	-6.3	8.1	—	—	-2.3

The free energies from Table I shows that at STP the most preferred structure is the on top adsorbed NH_2 for all 13Ns. For InN, the bridging NH_2 is almost as stable as the top adsorbed NH_2. The smaller difference in energy of the two NH_2 terminations for InN compared to AlN and GaN might stem from the larger distance between the neighboring groups causing the hydrogen bond formed to become elongated and weakened, not stabilizing the surface as much as for AlN and GaN.

The energy for the hollow-adsorbed NH is much higher than the NH_2 reconstructions as well as both the hollow and bridging N_2H_2 dimer. The large free energy difference between the NH adsorbed at a hollow site and the N_2H_2 dimers, around 100 kJ/mol, shows that the dimer is much preferred compared to the monomer at STP due the very strained geometry of the NH(ho) monomer. For only nitrogen the preferred reconstruction on AlN and GaN is the formation of dimers, with adsorption free energy much lower than an adsorbed N atom due to the strained structure of the monomer and presence of unpaired electrons on the lone N atom.

Most adsorption energies follow a trend were the adsorption energies increases as the metal moves downwards in group 13. Adsorption on AlN has the lowest standard energy of adsorbate formation, indicating that adsorption onto AlN is most preferred. On GaN, the energies are slightly higher by around 70 kJ/mol, compared to AlN. Continuing to InN, the adsorption energies are even higher than on GaN by around 50 kJ/mol, showing that adsorption on InN is least favorable. Adsorption of hydrogen deviates from the trend. The difference in adsorption energy of hydrogen between AlN and GaN is negligible, but the energy is much higher for InN. Hydrogen deviating from the trend is not too surprising since all other adsorptions modes forms a metal to nitrogen bond while hydrogen instead forms a metal to hydrogen bond. The In atom has a much larger radius compared to Al and Ga, this could cause the hydrogen to be pushed further away elongating the bond causing it to be less stable for In.

Equilibrium surface terminations

To create phase diagrams, we consider the different adsorption types as different surface species and we assume that the different surface species can form a homogeneous mixture on the surface, i.e., a 2D analogue of an ideal solution. A distinct surface one-phase region was

assumed to be the region where a certain set of surface species are present at significant amounts, arbitrarily set to at least 1 % of all surface species. The equilibrium amounts of each surface species was obtained from minimization of the systems Gibbs free energy at different combinations of temperature, total pressure, and initial composition.

Temperature-pressure phase diagrams were constructed between 200-1800 K and 0.001-1 bar total pressure to model a large set of possible conditions, containing the expected temperatures and pressures during CVD and ALD. A ratio of 1000:1 between gas and adsorption sites was used as an estimation of a surface covered by a free-flowing gas. The initial amount of NH_3 compared to N_2 in the gas was set to 2:15 and the surface was assumed initially to be bare.

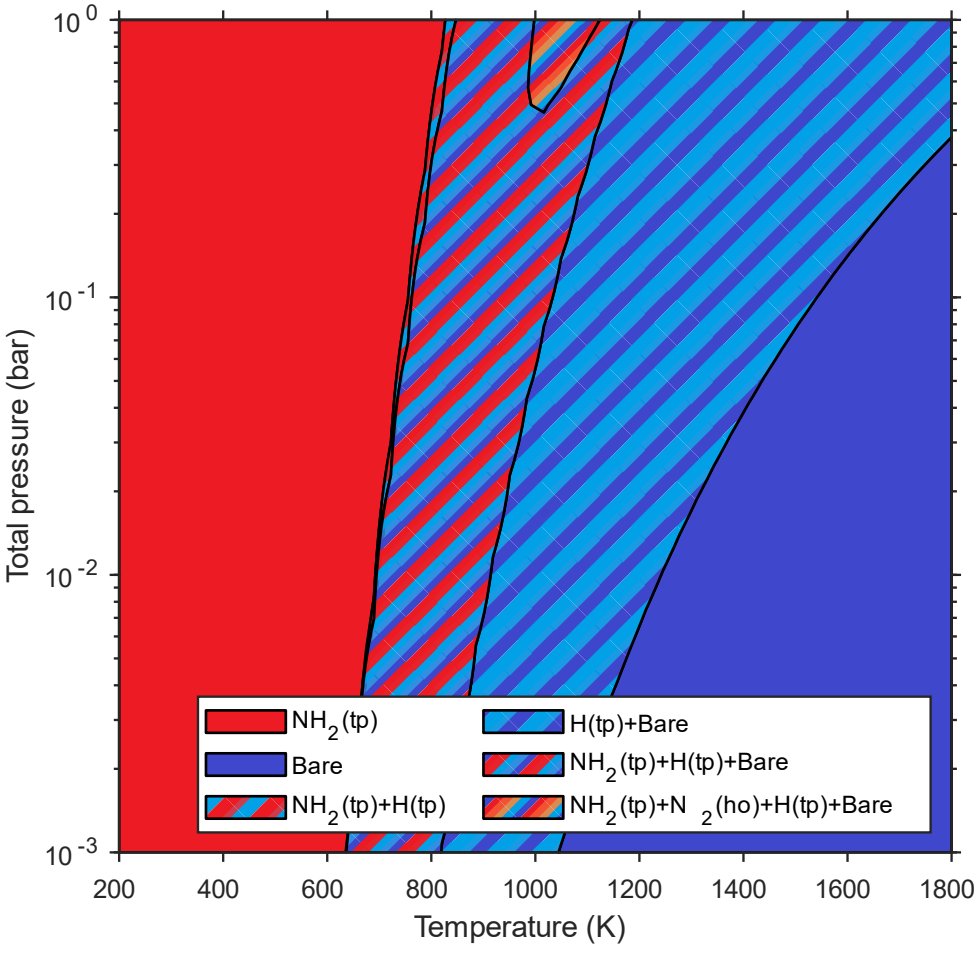

Figure 12. Temperature and pressure phase diagram for surface termination on AlN. Pure colored regions denote single species phases while striped regions denote multi species regions.

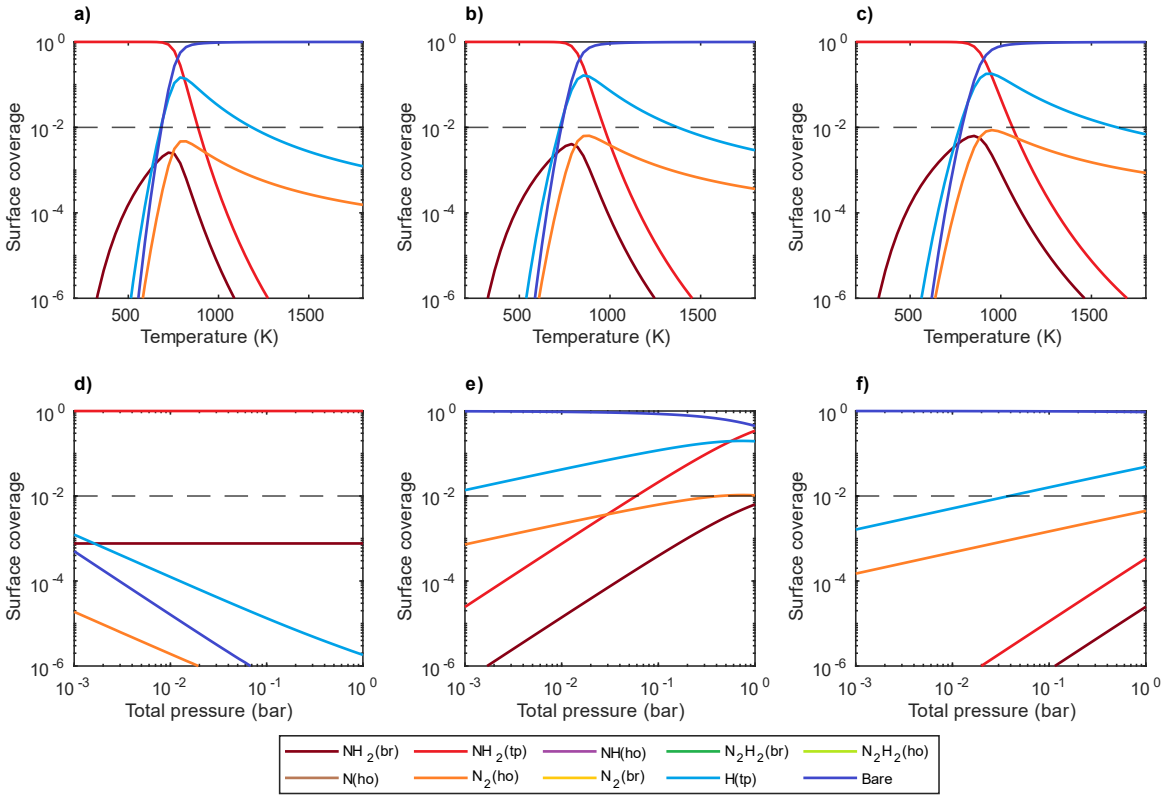

Figure 13. Surface coverage of NH_x terminations on AlN as a function of temperature at (a) 5.6 mbar, (b) 32 mbar and (c) 180 mbar and as a function of pressure at (d) 600 K, (e) 1000 K and (f) 1400 K.

The phase diagram for AlN, Figure 12, shows four dominating phases with the main species being NH_2(tp), H(tp) and bare sites. Both NH_2(tp) and bare surface reaches almost total coverage in the high and low temperature region respectively while the coverage for H(tp) quickly increases as temperature is increased and then taper of slowly as it is increased even more, Figure 13. The maximum coverage of H(tp) is pressure dependent and varies from around 10 % at 1 mbar to 20 % at 1 bar. At low temperatures, the surface is covered by a phase only consisting of NH_2(tp). This phase is stable up to 600 K at 1 mbar total pressure to around 700 K at 1 bar. Increasing the temperature above this phase transition line the surface switches to a phase containing H(tp) and bare sites as well as NH_2(tp). In a small transition region between those two phase-regions, there is a phase which does not contain any bare sites. The NH_2(tp), H(tp) and bare site phase is stable up to 800 K at 1 mbar to 1100 K at 1 bar. Higher temperatures cause NH_2(tp) termination to no longer be a favored termination and the surface becomes covered by a mixture of H(tp) and bare sites. At the highest temperature and lowest pressures all adsorptions become unfavorable, and the surface becomes bare. There is a small region of intermediate temperatures (900-1000 K) and high pressure (> 0.5 bar) where the surface

coverage of N_2(ho) dimer increases above the 1 % threshold. At slightly lower temperatures (850 K) the NH_2(br) reconstruction reaches it maximum coverage which at the highest pressures are just below the threshold of 1 %. Pressure has the effect of shifting the phase transitions unto higher temperatures and increasing the maximum surface coverage of the less abundant species.

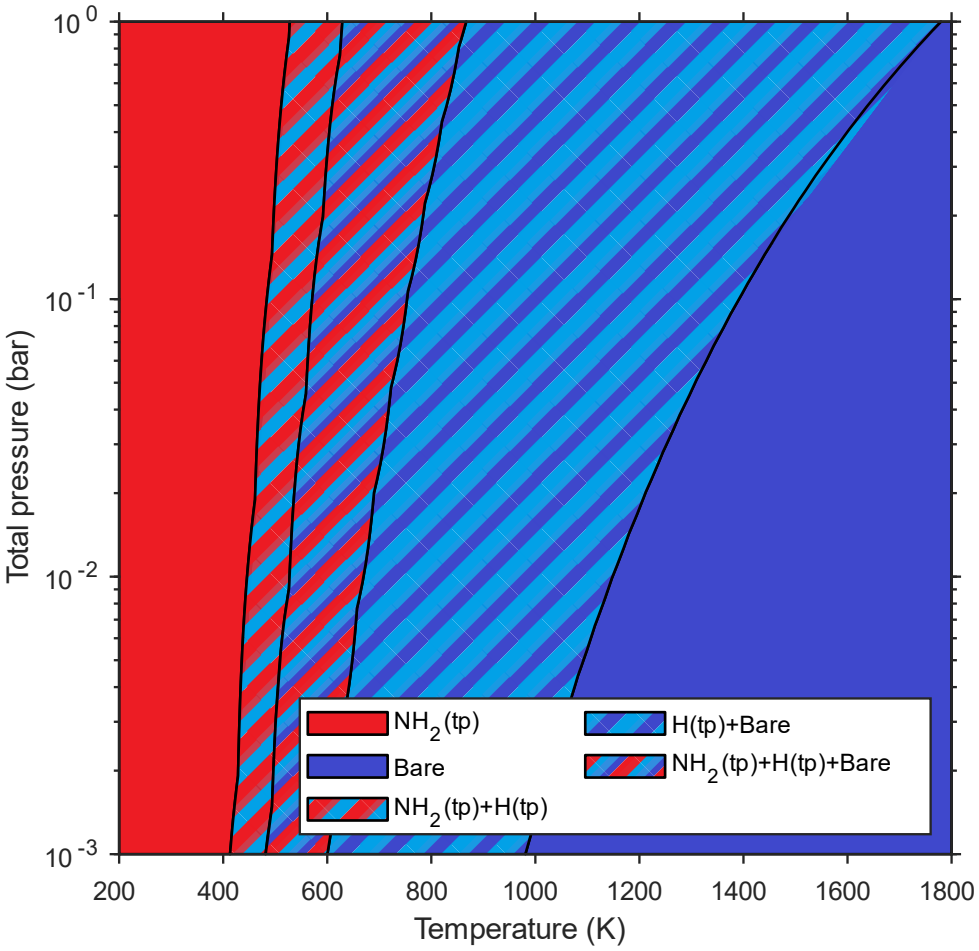

Figure 14. Temperature and pressure phase diagram for surface termination on GaN. Pure colored regions denote single species phases while striped regions denote multi species regions.

For GaN, the phase diagram, Figure 14, looks similar to that of AlN with some slight differences. The main dominating terminations are again NH_2(tp), H(tp) and bare sites. The phase diagram contains the same dominating phases regions with the addition of the transition phase (NH_2(tp) + H(tp)) between the NH_2(tp) phase and (NH_2(tp) + H(tp) + bare) phase being much more pronounced. The phase transitions occur at lower temperatures compared to AlN, the transition of NH2(tp) into (NH_2(tp) + H(tp)) start at 450 K at 1 mbar to 500 K at 1 bar. Bare

sites start to form around 480 K at low pressures and 600 K at atmospheric pressure. NH_2(tp) disappears around 600-800 K and H(tp) finally disappears above 1000-1500 K. There are some differences in the less abundant reconstructions compared to AlN, all other reconstructions reach much lower maxima compared to those on AlN, around 0.1 % for NH_2(br) and N_2(br), Figure S11.

InN on the other hand exhibit a quite different phase diagram, Figure 15. At most of the investigated temperatures, above 300-450 K, the only stable structure is the bare surface. At low temperatures there are, however, three regions containing other terminations. At the lowest temperatures and intermediate to high pressure, the surface is a mixture of the two adsorbed NH_2 species. When increasing the temperature bare sites starts to form and are mixed into the phase. Above 250-330 K NH_2(br) decreases below the threshold and after 300-450 K NH_2(tp) also falls below the 1 % mark. A similarity of the InN phase diagram with those for AlN and GaN is that NH_2(tp) has almost total coverage at low temperatures and bare sites at high temperatures. NH_2(br) rises above the threshold just after 200 K and reaches its maximum coverage of 1-2 % before quickly falling back below the threshold. The lower adsorption energy for hydrogen on InN causes the maximum H(tp) coverage to be well belove the threshold at around 0.001-0.01 %, Figure S12.

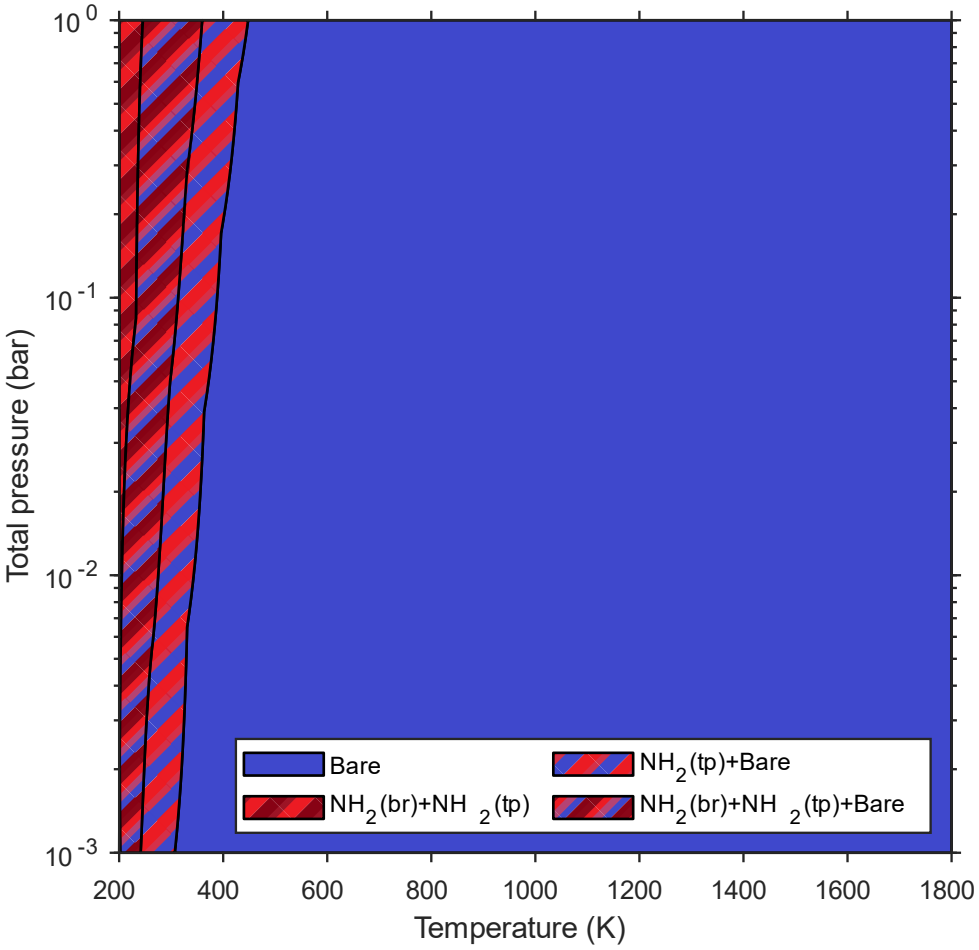

Figure 15. Temperature and pressure phase diagram for surface termination on InN. Pure colored regions denote single species phases while striped regions denote multi species regions.

A limitation of the equilibrium model is that it predicts the full decomposition of NH_3 into N_2 and H_2 at higher temperatures. According to recent kinetic simulations, this decomposition is too slow to occur during CVD or ALD [9]. This would lead to a too low amount of NH_3 in the gas and change the surface phase diagrams. To solve this problem additional pseudo-equilibrium calculations were performed with N_2 excluded from the possible decomposition products of NH_3. N_2 is kept as a carrier gas and is allowed to adsorb as N_2 dimers but not decompose or abstract hydrogen.

The removal of decomposition to N_2 changes the phase diagrams significantly as expected. For AlN, Figure 16, the main surface structures are still NH_2(tp), H(tp) and bare sites with the addition of NH_2(br) at intermediate temperatures. At low temperatures NH_2(tp) still dominates the surface coverage up to 890 K where NH_2(br) appears. Bare sites start to appear at higher

temperatures as the nitrogen from NH_3 cannot desorb as nitrogen gas, causing more sites to be occupied. At the highest temperatures however, bare sites start to dominate, and the surface becomes uncovered. As less NH_3 decomposes there is less free hydrogen present in the system, which leads to the H(tp)-containing phases to only appear in a small area of high temperature and pressure. Other minor species that appear are the N_2H_2(ho) and NH(ho) who reach their maximum below 0.1 % coverage at intermediate temperatures, Figure S13.

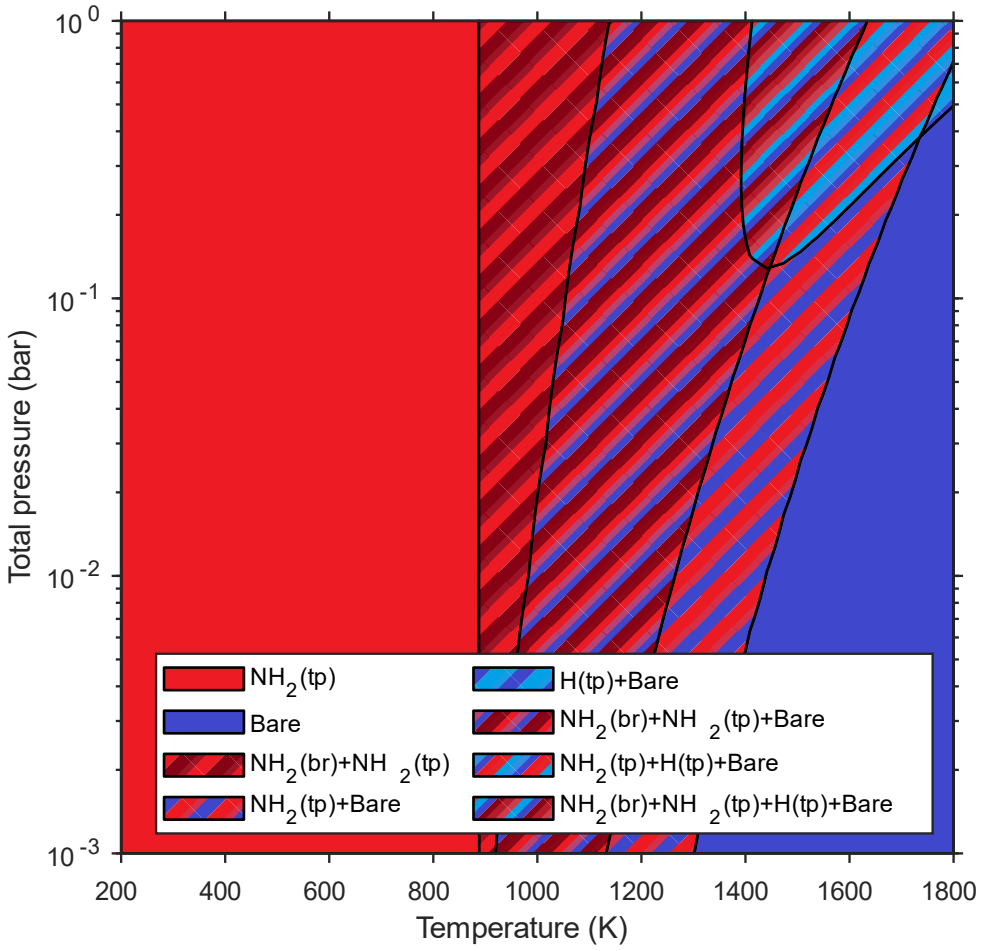

Figure 16. Left, temperature and pressure phase diagram for surfaces reconstructions on AlN with decomposition to N_2 removed. Right, surface coverage at constant pressure along the lines marked in the phase diagram.

The phase diagram of GaN shows alterations as that of AlN when excluding the NH_3 decomposition process, Figure17. At low temperatures NH_2(tp) is the only significant structure up to about 600 K. Bare sites starts to appear as temperature is increased and in a small phase transition region only NH_2(tp) and bare sites are present above 1 %. As temperature is raised

further, the two N_2H_2 structures appear, first the bridging then the hollow, for intermediate temperatures before starting to drop again. The N_2H_2 and NH_2(tp) structures drops below the 1 % threshold almost at the same temperature and at high temperatures only bare sites are stable. For a large span of intermediate temperature the coverage of H(tp) is just below the threshold, and only at the highest temperatures does it climb above it, Figure S14.

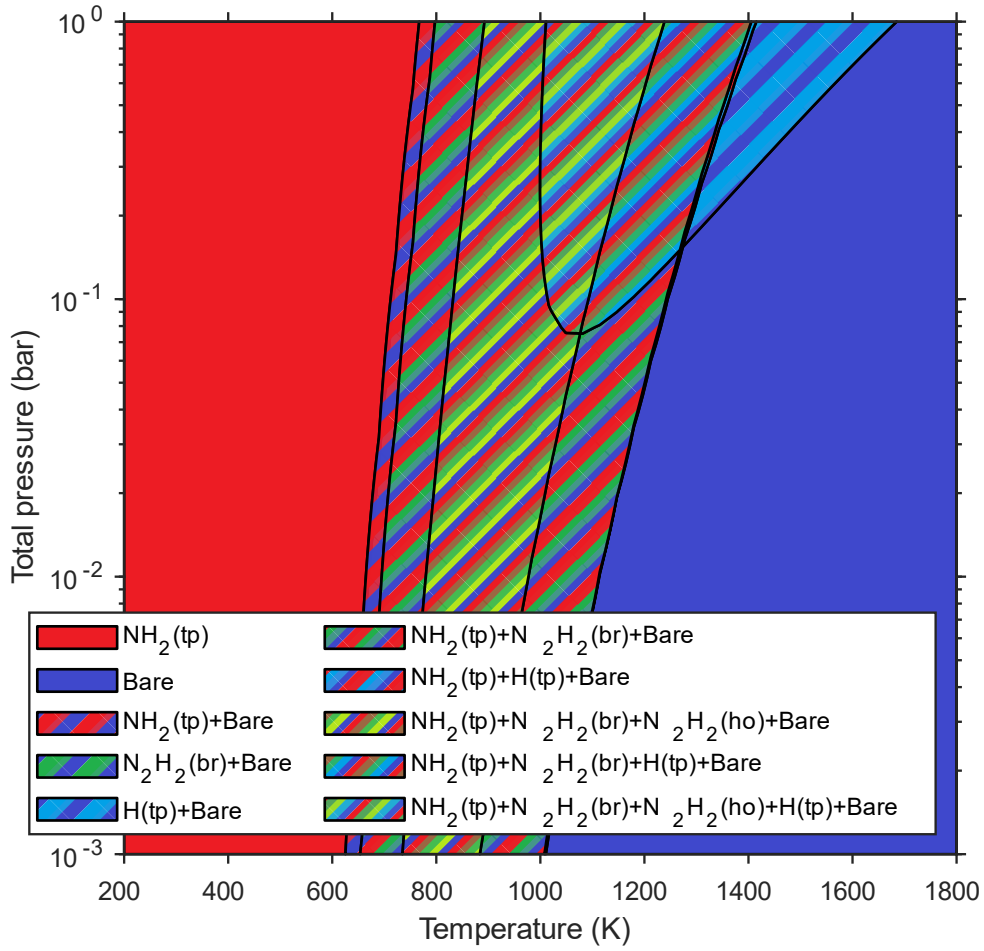

Figure 17. Left, temperature and pressure phase diagram for surfaces reconstructions on GaN with decomposition to N_2 removed. Right, surface coverage at constant pressure along the lines marked in the phase diagram.

For InN the phase diagram, Figure 18, without NH_3 decomposition exhibits fewer phases compared to those of AlN and GaN, as in the case with NH_3 decomposition included (Figure 15). At low temperatures, the surface is covered by a mixture of NH_2(tp) and bare sites. There is a region at high pressure and low temperature where NH_2(br) also reaches above the threshold. The NH_2(tp) is stable up to slightly higher temperatures compared to if

decomposition was allowed, until bare sites become the only stable structure. The two most abundant minor structures were the two N_2H_2 dimers with a maximum of around 0.1-0.2 % at around 600 K, Figure S15.

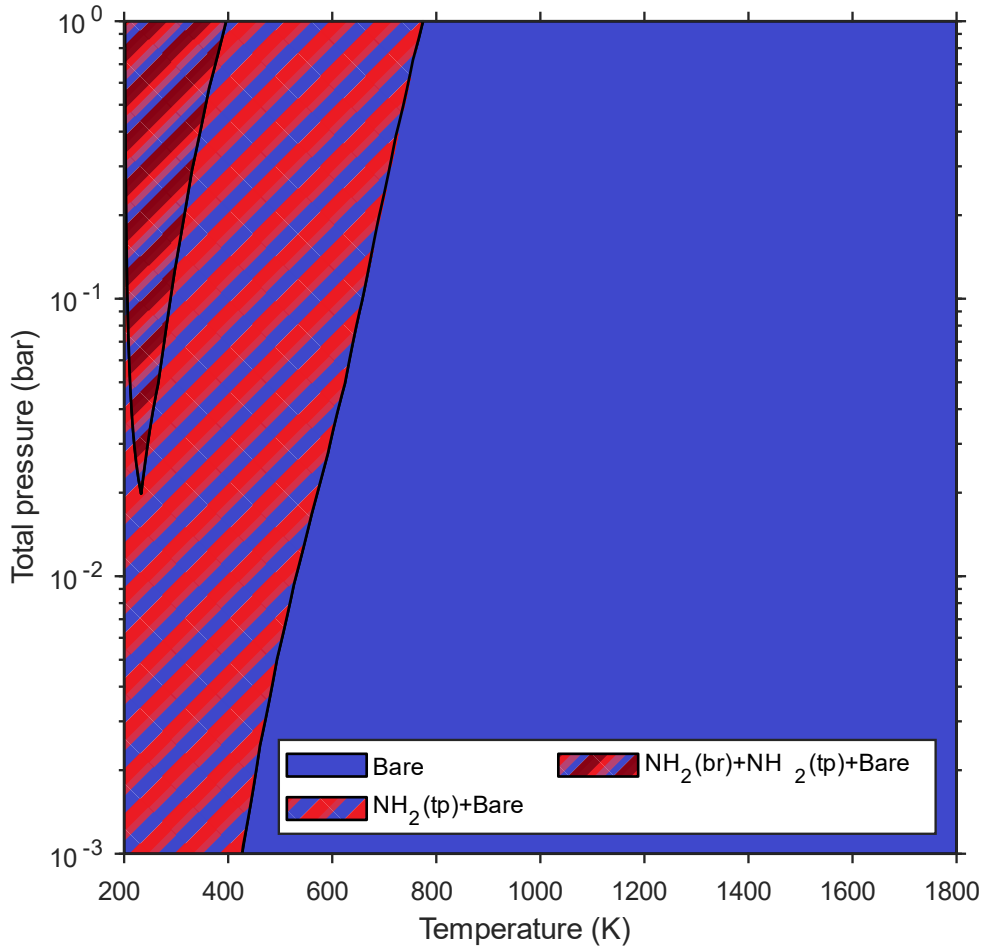

Figure 18. Left, temperature and pressure phase diagram for surfaces reconstructions on InN with decomposition to N_2 removed. Right, surface coverage at constant pressure along the lines marked in the phase diagram.

Ternary phase diagrams

Ternary phase diagrams were constructed to investigate the effect on the surface termination at various ratios of N_2 and NH_3 in the gas as well as the ratio of gas molecules to the number of surface sites. The phase diagrams were constructed by minimizing of the Gibbs energy at a set temperatures and pressures and by varying the initial amount of NH_3, N_2 and number of surface sites, keeping the total amount constant. Since CVD and ALD usually utilizes a flowing gas

over a small substrate the main region of interest of these ternary diagrams is where the ratio of surface sites to gas molecules approaches 0.

The ternary phase diagram for AlN, Figure 19, shows that the surface termination depends only weakly on the composition. Only in a few cases does a slight change in composition change the preferred termination. The largest phase region at low temperature and pressure is the phase dominated almost exclusively by NH_2(tp). This phase is the preferred phase if there are enough NH_3 molecules in the gas phase to saturate the whole surface and other phases only start to appear when the amount of NH_3 is too low. At high temperature and pressures the phase diagram is instead dominated by a large region of a mixed phase of NH_2(tp), H(tp) and bare sites. In the limit of low surface to gas ratio, corresponding to experimental conditions during CVD and ALD, both phase diagrams only show a single phase, except when the amount of NH_3(g) vanishes where the lack of hydrogen causes the surface to form other terminations.

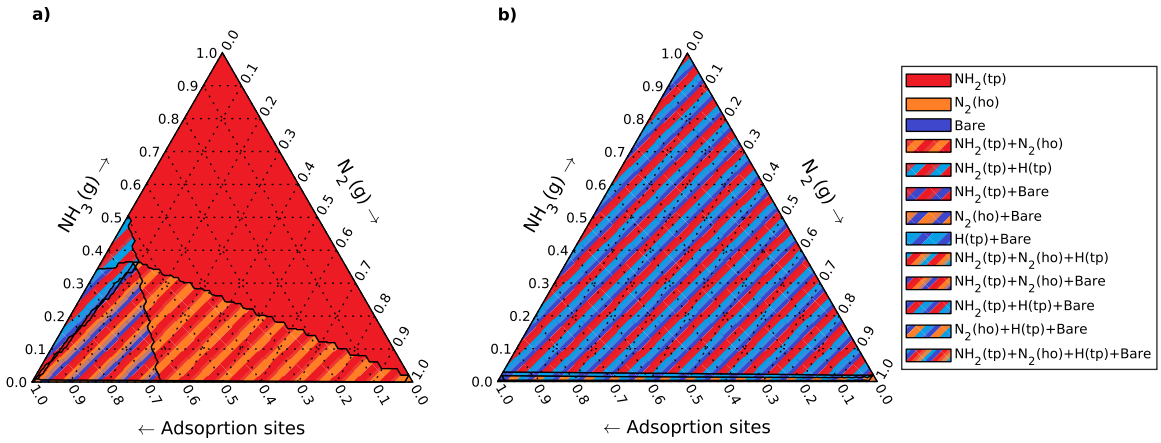

Figure 19. Ternary phase diagram for NH_x surface terminations of AlN at (a) 5.6 mbar, 200 K and (b) 180 mbar, 1000 K. Solid colors denote single-species phases and striped regions denote multi-specie phases.

The ternary phase diagram for GaN shows many similarities to that of AlN, in the low temperature and pressure case, Figure S16. The main difference is the absence of phases containing N_2 surface dimers. At high temperature and pressure, the surface becomes covered by a mix of H(tp) and bare sites terminations at all compositions under the condition that there is enough hydrogen present in the system. InN also show similarities with AlN and GaN in the low temperature limit, Figure S17. Most of the compositions yields a large NH_2(tp) phase for

many and the main difference is the absence of H(tp) containing phases as the amount of NH_3 is lowered, since this termination is much less preferred on InN compared to on the other surfaces. At high temperatures the surface becomes bare, with no other phases for any initial compositions.

Discussion

In general, the different 13Ns show similar structures upon adsorption of N_xH_y and the energies follow similar trends. At low temperatures, the surfaces are terminated by relatively undecomposed adsorbates with the hydrogen-bonded NH_2(tp) termination being the most stable surface structure. At higher temperatures the entropy causes the surface to prefer structures that lead to more free gas molecules such as either N_2H_2 and N_2 dimer adsorbed species and at the highest temperatures the surface becomes uncovered forming bare metal sites.

There is a clear decrease of NH_x coverage when traversing down the 13Ns by increasing the atomic number of the metal. AlN is covered by nitrogen-containing terminations in a much larger temperature and pressure range compared to GaN which in turn is much more covered compared to InN. This would in turn lead to a much less favored CVD or ALD process for InN since much less of the supplied NH_3 would bind to the surface to facilitate film growth. From the literature on experimental studies of 13N deposition by CVD and ALD, it is clear that InN is more challenging to deposit than AlN and GaN.

The lack of adsorption onto InN can be explained by the low reactivity of ammonia onto the surface. At temperatures above 320 K at CVD and ALD pressures even the most stable termination, NH_2(tp), is less thermodynamically stable than ammonia in gas phase at normal pressures and bare In sites. According to the HSAB theory In is, compared to Al and Ga, a soft acid while the nitrogen in ammonia is a hard base [24]. As hard bases prefer to react with hard acids and soft bases prefer soft acids, ammonia would prefer to react with the harder acid Al or Ga than with In. This is also shown in the ratio of NH_3 to 13-precursor used in CVD of 13Ns, where AlN requires a ratio of around 100, GaN a ratio of 1000 and InN a ratio of up to 100 000.

The high stability of N_2 and H_2 gas at equilibrium causes the surface to become uncovered at higher temperatures. This is a challenge for the CVD and ALD growth as the surfaces would decompose during a high temperature process if enough time is passed. This equilibrium decomposition is most noticeable for InN where the surface is bare already at room temperature, a temperature much lower than the one needed for CVD and ALD growth. Overcoming this problem leads to the need to shift the process from the thermal equilibrium, either by not

allowing enough time for the NH_x to decompose into N_2 and H_2 or by using a plasma enhanced process.

Conclusions

Structures and energies of different NH_x surface structures on the three 13Ns, AlN, GaN and InN were investigated by DFT. Their stability at different temperature and pressures were determined by a minimization of the systems Gibbs energy. We have shown that the surface terminations are dependent on temperature with a hydrogen bonding NH_2(tp) surface structure being the dominating structure at low temperatures and a bare surface being dominating at high temperatures for all three 13Ns. The NH_2(tp) surface structure forms a good candidate for growth of 13Ns films since the availability of lone electrons pairs on the surface nitrogen can act as adsorption sites for a metal precursor containing a Lewis-acidic metal-atom. We also show that stability of the nitrogen containing surface structures decreases as the atomic number of the metal moves downwards in group 13, indicating that the growth process would be easier on AlN compared to GaN and hardest on InN, in agreement with experimental findings. The obtained structures can also be used to further develop models to investigate the atomistic processes during CVD and ALD growth as a basis for the adsorption mechanics of a metal precursors.

Supporting information

Figures of the surface structures for all 13Ns, surface coverages on GaN and InN as functions of temperature and pressure, and ternary phase diagrams for GaN and InN are available in the supporting information.

Acknowledgements

This project was funded by the Swedish foundation for Strategic Research through the project “Time-resolved low temperature CVD for III-nitrides” (No. SSF-RMA 15-0018). L.O. acknowledges financial support from the Swedish Government Strategic Research Area in Materials Science on Functional Materials at the Linköping University (Faculty Grant SFO Mat LiU No. 2009 00971) and from the Swedish Research Council (VR). Supercomputing resources were provided by the Swedish National Infrastructure for Computing (SNIC) and the Swedish National Supercomputer Centre (NSC).

References

1. Ambacher O. Growth and applications of group III-nitrides. J Phys D Appl Phys. 1998 Oct 21;31(20):2653–710.
2. Guo Q, Yoshida A. Temperature Dependence of Band Gap Change in InN and AlN. Jpn J Appl Phys. 1994 May 1;33(5R):2453.
3. Davydov VY, Klochikhin AA, Emtsev V V., Ivanov S V., Vekshin V V., Bechstedt F, et al. Band gap of InN and In-rich $In_xGa_{1-x}N$ alloys ($0.36 < x < 1$). Phys Status Solidi Basic Res. 2002 Apr 1;230(2):R4–6.
4. Bougrov V, Levinshtein M, Rumyantsev S, Zubrilov A. Gallium Nitride (GaN). In: Levinshtein M, Rumyantsev S, Shur M, editors. Properties of Advanced Semiconductor Materials: GaN, AIN, InN, BN, SiC, SiGe. New York: John Wiley & Sons, Inc; 2001. p. 1–30.
5. Amano H, Sawaki N, Akasaki I, Toyoda Y. Metalorganic vapor phase epitaxial growth of a high quality GaN film using an AlN buffer layer. Appl Phys Lett. 1998 Aug 4;48(5):353.
6. Nakamura S. Gan growth using gan buffer layer. Jpn J Appl Phys. 1991 Oct 1;30(10A):L1705–7.
7. Bhuiyan AG, Hashimoto A, Yamamoto A. Indium nitride (InN): A review on growth, characterization, and properties. J Appl Phys. 2003 Aug 19;94(5):2779.
8. Bellotti E, Doshi BK, Brennan KF, Albrecht JD, Ruden PP. Ensemble Monte Carlo study of electron transport in wurtzite InN. J Appl Phys. 1998 Dec 29;85(2):916.
9. Rönnby K, Pedersen H, Ojamäe L. Kinetic modeling of ammonia decomposition at chemical vapor deposition conditions. J Vac Sci Technol A. 2020 Aug 10;38(5):050402.
10. Hsu CW, Deminskyi P, Martinovic I, Ivanov IG, Palisaitis J, Pedersen H. Direct epitaxial nanometer-thin InN of high structural quality on 4H-SiC by atomic layer deposition. Appl Phys Lett. 2020 Sep 1;117(9):093101.
11. Hsu CW, Deminskyi P, Persson A, Karlsson M, Pedersen H. On the dynamics in chemical vapor deposition of InN. J Appl Phys. 2021 Oct 4;130(13):135302.
12. Bui KM, Iwata JI, Kangawa Y, Shiraishi K, Shigeta Y, Oshiyama A. Reaction Pathway of Surface-Catalyzed Ammonia Decomposition and Nitrogen Incorporation in Epitaxial Growth of Gallium Nitride. J Phys Chem C. 2018 Nov 1;122(43):24665–71.
13. Cardelino BH, Cardelino CA. Dissociative chemisorption of trimethylgallium, trimethylindium, and ammonia on gallium and indium nitride substrates. A computational study. J Phys Chem C. 2011 May 12;115(18):9090–104.
14. Walkosz W, Zapol P, Stephenson GB. A DFT study of reaction pathways of NH_3 decomposition on InN (0001) surface. J Chem Phys. 2012 Aug 2;137(5):054708.

15. Kresse G, Hafner J. Ab initio molecular dynamics for liquid metals. Phys Rev B. 1993 Jan 1;47(1):558–61.

16. Kresse G, Furthmüller J. Efficiency of ab-initio total energy calculations for metals and semiconductors using a plane-wave basis set. Comput Mater Sci. 1996 Jul 1;6(1):15–50.

17. Kresse G, Furthmüller J. Efficient iterative schemes for ab initio total-energy calculations using a plane-wave basis set. Phys Rev B. 1996 Oct 15;54(16):11169–86.

18. Sheppard D, Terrell R, Henkelman G. Optimization methods for finding minimum energy paths. J Chem Phys. 2008 Apr 2;128(13):134106.

19. Perdew JP, Burke K, Ernzerhof M. Generalized gradient approximation made simple. Phys Rev Lett. 1996 Oct 28;77(18):3865–8.

20. Grimme S, Antony J, Ehrlich S, Krieg H. A consistent and accurate ab initio parametrization of density functional dispersion correction (DFT-D) for the 94 elements H-Pu. J Chem Phys. 2010 Apr 16;132(15):154104.

21. Kresse G, Joubert D. From ultrasoft pseudopotentials to the projector augmented-wave method. Phys Rev B. 1999 Jan 15;59(3):1758–75.

22. Togo A, Tanaka I. First principles phonon calculations in materials science. Scr Mater. 2015 Nov 1;108:1–5.

23. An Q, Jaramillo-Botero A, Liu WG, Goddard WA. Reaction pathways of GaN (0001) growth from trimethylgallium and ammonia versus triethylgallium and hydrazine using first principle calculations. J Phys Chem C. 2015 Feb 26;119(8):4095–103.

24. Jolly WL. Modern Inorganic Chemistry. New York: McGraw-Hill; 1984. (International student edition).